Journal of Applied Fluid Mechanics, Vol. 7, No. 3, pp. 447-458, 2014.
Available online at www.jafmonline.net, ISSN 1735-3572, EISSN 1735-3645.

Diffusion-Thermo and Thermal-diffusion Effects on MHD Visco-Elastic Fluid Flow over a Vertical Plate

D. Yasmin[1], T.Ahmed[1], N. N. Anika[1], M. M. Mukitul Hasan[2], and M. Mahmud Alam[1†]

[1] *Mathematics Discipline, Khulna University, Khulna-9208, Bangladesh*
[2] *Department of Mathematics, Khulna Public College, Khulna-9000, Bangladesh*

†Corresponding Author Email: *alam_mahmud2000@yahoo.com*

(Received March 17, 2013; accepted June 9, 2013)

ABSTRACT

Unsteady MHD visco-elastic fluid flow has been studied numerically under the action of transverse magnetic field with diffusion-thermo and thermal diffusion for small magnetic Reynolds number. The governing equations are non-dimensionalized by usual non-dimensional variables. The obtained equations are solved by explicit finite difference technique. The solutions of the dimensionless velocity, temperature and concentration equations are shown graphically. The effects of parameters on the shear stress, Nusselt number and Sherwood number are discussed in graphical form. Finally, a qualitative comparison with previous work is tabulated.

Keywords: MHD, Visco-elastic Fluid, Heat and Mass.

1. INTRODUCTION

The mixed convection boundary layer flow of non-Newtonian fluid in the presence of strong magnetic field has wide range of application in nuclear engineering and industries. In astrophysical and geophysical studies, the MHD boundary layer flows of an electrically conducting fluid have also enormous applications. Many researchers have studied the transient laminar natural convection flow past a vertical porous plate for the application in the branch of science and technology such as in the field of agriculture engineering and chemical engineering. In petroleum refineries, movement of oil, water and gas through porous media for purification and filtration are bright applied areas of research. With the advancement of science and technology, MHD study on any fluid flow phenomenon exhibits some results which have constructive application for the design of devices. MHD heat transfer has great importance in the liquid metal flows, ionized gas flow in a nuclear reactor and electrolytes. Research works on radiation of heat in natural convection flow are very limited, though these have many modern applications viz. missile technology used in army, nuclear power plant, parts of aircraft and ceramic tiles.

Heat and mass transfer in non-Newtonian fluids is of great interest in many operations in the chemical and process engineering industries including coaxial mixers, blood oxygenators, milk processing, steady-state tubular reactors, and capillary column inverse gas chromatography devices, mixing mechanisms, bubble-drop formation processes , dissolution processes, and cloud transport phenomena. Many geometrical configurations have been addressed including flat plates, channels, cones, spheres, wedges, inclined planes, and wavy surfaces. Non-Newtonian heat transfer studies have included power-law fluid i.e. shear-thinning and shear thickening fluids, simple viscoelastic fluids, Criminale-Ericksen-Fibley viscoelastic fluids, Johnson-Segalman rheological fluids, Bingham yield stress fluids, second grade (Reiner-Rivlin) viscoselastic fluids, third grade viscoelastic fluids, and bi-viscosity rheological fluids. Viscoelastic properties can enhance or depress heat transfer rates, depending upon the kinematic characteristics of the flow field under consideration and the direction of heat transfer. Firstly for such a fluid considering the oscillatory two-dimensional viscoelastic flow along an infinite porous wall, showing that an increase in the Walters elasticity parameter and the frequency parameter reduces the phase of the skin-friction has been investigated by Soundalegkar and Puri (1969). The laminar flow of an electrical-conducting Walter's liquid, past an infinite non-conducting vertical plate for impulsive as well as uniformly accelerated motion of the plate has been presented by Samria *et al*. (1990), in the presence of a transverse magnetic field. The Unsteady magnetohydrodynamic flows in a rotating elasto-viscous fluid have been analyzed by Nanousis (1992). The MHD free convection flow of

a visco-elastic fluid past a vertical porous plate has been investigated by Chowdhury and Islam (2000). Recently, the effects of thermal radiation on unsteady free convection flow of an elasto-viscous fluid over a moving vertical plate with variable temperature in the presence of magnetic field through porous medium have been studied be Rajesh and Varma (2010). The analytical study of Heat source and mass transfer effects on MHD free convection flow of a visco-elastic fluid past an exponentially accelerated infinite vertical plate with variable temperature through porous medium has been investigated by Rakesh Kumar *et al*. (2011).

The heat and mass transfer occur simultaneously between the fluxes, the driving potentials are of more intricate nature. An energy flux can be generated not only by temperature gradients but by composition gradients. The energy flux caused by a composition is called Dufour or diffusion-thermo effect. Temperature gradients can also create mass fluxes, and this is the Soret or thermal-diffusion effect. Generally, the thermal-diffusion and the diffusion-thermo effects are of smaller-order magnitude than the effects prescribed by Fourier's or Fick's laws and are often neglected in heat and mass transfer processes. The thermal-diffusion effect, for instance, has been utilized for isotope separation and in mixture between gases with very light molecular weight (H_2, He) and of medium molecular weight (Nitrogen-air) the diffusion-thermo effect was found to be of a magnitude such that it cannot be neglected. Many transport processes can be found in various ways in both nature and technology, in which the combined heat and mass transfer occur due to buoyancy forces caused by thermal diffusion and mass diffusion. Some of the convective heat and mass transfer processes with phase change include the evaporation of liquid at the interface between a gas and liquid or the sublimation at a solid-gas interface. The process of mass transfer affects all separation processes in chemical engineering such as the drying of solid materials, distillation, extraction and absorption. Heat and mass transfer for Soret and Dufour effect on mixed convection boundary layer flow over a stretching vertical surface in a porous medium filled with a viscoelastic fluid has been analyzed by Hayat *et al*. (2010). The steady mixed convection boundary layer flow due to the combined effect of heat and mass transfer over a stretched vertical surface in a porous medium filled with a viscoelastic fluid under Soret and Dufour effects in the presence of magnetic field has been investigated by Gbadeyan *et al*. (2011). Mixed convective MHD flow of visco-elastic fluid past a vertical infinite plate with mass transfer in the presence of magnetic field has been studied by Mahanta and Choudhury (2012). MHD unsteady memory convective flow through porous medium with variable suction has been studied by Hussaini *et al*. (2013).

The objective of this study is to extend the work of Mahanta and Choudhury (2012) with visco-elastic flow characterized by second-order fluid as MHD free convection and mass transfer visco-elastic fluid flow in vertical porous plate with mass diffusion and thermal diffusion. The governing equations involved in this problem have been transformed into non-similar coupled partial differential equations by usual transformations. The problem has been solved by explicit finite difference method. Finally, the comparison of the present results with the results of Gbadeyan *et. al*. (2011) has been shown in tabular form.

2. MATHEMATICAL FORMULATION

Consider an unsteady MHD visco-elastic (Walters's liquid B') mixed convective heat and mass transfer flow of an incompressible, electrically conducting viscous fluid past an electrically nonconducting isothermal impulsive vertical plate. The positive x coordinate is measured along the plate in the direction of fluid motion and the positive y coordinate is measured normal to the plate. A uniform transverse magnetic field of magnitude B_0 is applied in the direction of $y-$axis . Initially, it is considered that the plate as well as the fluid is at the same temperature $T(=T_\infty)$ and concentration level $C(=C_\infty)$. Also it is assumed that the temperature of the plate and concentration are raised to $T_w(>T_\infty)$ and $C_w(>C_\infty)$ respectively, which are there after maintained constant, where T_w, C_w are temperature and concentration at the wall and T_∞, C_∞ are the temperature and concentration of the species outside the boundary layer respectively. The physical configuration of the problem is furnished in Fig. 1.

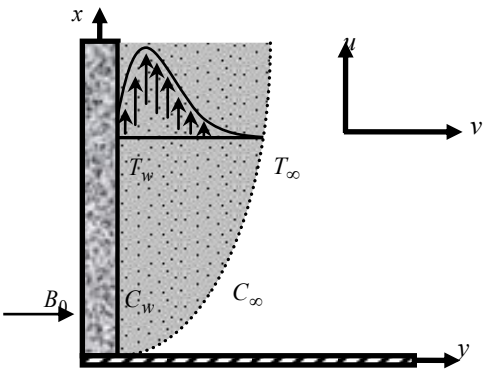

Fig. 1. Physical configuration and coordinate system.

The magnetic Reynolds number of the flow is taken to be small enough and the magnetic field is negligible in comparison with applied magnetic field and the magnetic lines are fixed relative to the fluid. Using the relation $\nabla\cdot\mathbf{J}=0$ for the current density $\mathbf{J}=(J_x,J_y,J_z)$ where $J_y=$constant . Since the plate is nonconducting, $J_y=0$ at the plate and hence zero everywhere.

Within the framework of the above-stated assumptions the generalized equations relevant to the unsteady problem are governed by the following system of coupled partial differential equations as;

The Continuity equation;

$$\frac{\partial u}{\partial x}+\frac{\partial v}{\partial y}=0 \tag{1}$$

The Momentum equation;

$$\frac{\partial u}{\partial t}+u\frac{\partial u}{\partial x}+v\frac{\partial u}{\partial y}=\upsilon_1\frac{\partial^2 u}{\partial y^2}-\frac{\sigma B_0^2 u}{\rho}+gB_T\left(T-T_\infty\right)$$

$$+gB_C\left(C-C_\infty\right)+\upsilon_2\left\{\frac{\partial^2}{\partial y^2}\left(\frac{\partial u}{\partial t}\right)+v\frac{\partial^3 u}{\partial y^3}\right\} \tag{2}$$

The Energy equation;

$$\frac{\partial T}{\partial t}+u\frac{\partial T}{\partial x}+v\frac{\partial T}{\partial y}=\frac{\kappa}{\rho c_p}\frac{\partial^2 T}{\partial y^2}+\frac{Dk_t}{c_s c_p}\frac{\partial^2 C}{\partial y^2} \tag{3}$$

The Concentration equation;

$$\frac{\partial C}{\partial t}+u\frac{\partial C}{\partial x}+v\frac{\partial C}{\partial y}=D\frac{\partial^2 C}{\partial y^2}+\frac{Dk_t}{T_m}\frac{\partial^2 T}{\partial y^2} \tag{4}$$

corresponding boundary conditions are;

$$u=U_\infty,\ v=0,\ T=T_w,\ C=C_w \quad \text{at } y=0$$

$$u=0,\ v=0,\ T\to T_\infty,\ C\to C_\infty \quad \text{as } y\to\infty \tag{5}$$

where u and v are the x and y components of velocity vector, σ is the electric conductivity, υ_1, υ_2 are the kinematic coefficient viscosity, ρ is the density of the fluid, κ is the thermal conductivity, c_p is the specific heat at the constant pressure , D is the coefficient of mass diffusivity, k_t is the thermal diffusion ratio, c_s is the concentration susceptibility, T_m is the mean fluid temperature, β_T is the co-efficient of volumetric expansion for heat transfer, β_C is the co-efficient of volumetric expansion for mass transfer.

To obtain the governing equations and the boundary condition in dimension less form, the following non-dimensional quantities are introduced as;

$$X=\frac{xU_\infty}{\upsilon_1},\quad Y=\frac{yU_\infty}{\upsilon_1},\quad U=\frac{u}{U_\infty},\quad V=\frac{v}{U_\infty},$$

$$\tau=\frac{tU_\infty^2}{\upsilon},\ \theta=\frac{T-T_\infty}{T_w-T_\infty}\ \text{and}\ \varphi=\frac{C-C_\infty}{C_w-C_\infty}.$$

Substituting the above dimensionless variables in Eqs .(1) to (4) and corresponding boundary conditions (5), the obtained dimensionless coupled non-linear partial differential equations are;

$$\frac{\partial U}{\partial X}+\frac{\partial V}{\partial Y}=0 \tag{6}$$

$$\frac{\partial U}{\partial \tau}+U\frac{\partial U}{\partial X}+V\frac{\partial U}{\partial Y}=\frac{\partial^2 U}{\partial Y^2}+G_r\,\theta+G_m\phi-MU$$

$$+\alpha\left\{\frac{\partial^2}{\partial Y^2}\left(\frac{\partial U}{\partial \tau}\right)+V\frac{\partial^3 U}{\partial Y^3}\right\} \tag{7}$$

$$\frac{\partial \theta}{\partial \tau}+U\frac{\partial \theta}{\partial X}+V\frac{\partial \theta}{\partial Y}=\frac{1}{P_r}\frac{\partial^2 \theta}{\partial Y^2}+D_u\frac{\partial^2 \phi}{\partial Y^2} \tag{8}$$

$$\frac{\partial \varphi}{\partial \tau}+U\frac{\partial \varphi}{\partial X}+V\frac{\partial \varphi}{\partial Y}=S_r\frac{\partial^2 \phi}{\partial Y^2}+\frac{1}{S_c}\frac{\partial^2 \theta}{\partial Y^2} \tag{9}$$

boundary conditions are;

$$U=1,\ V=0,\ \theta=1,\ \phi=1 \text{ at } Y=0$$

$$U=0,\ W=0,\ \theta=0,\ \phi=0 \text{ as } Y\to\infty \tag{10}$$

where τ represents the dimensionless time, X and Y are the dimensionless Cartesian coordinates, U is the dimensionless velocity, θ is the dimensionless temperature, ϕ is the dimensionless concentration,

$G_r=\dfrac{gB_T\left(T_w-T_\infty\right)\upsilon_1}{U_\infty^3}$ (Grashof Number),

$G_m=\dfrac{gB_C\left(C_w-C_\infty\right)\upsilon_1}{U_\infty^3}$ (Modified Grashof Number), $\alpha=\dfrac{\upsilon_2}{\upsilon_1}U_\infty^2$ (Visco-elastic Parameter),

$M=\dfrac{\sigma B_0^2\upsilon}{\rho U_\infty^2}$ (Magnetic Parameter), $P_r=\dfrac{\rho c_p\upsilon}{\kappa}$ (Prandtl Number), $D_u=\dfrac{Dk_t}{\upsilon_1 c_s c_p}\dfrac{\left(C_w-C_\infty\right)}{\left(T_w-T_\infty\right)}$ (Dufour Number), $S_c=\dfrac{\upsilon_1}{D}$ (Schmidt Number) and $S_r=\dfrac{Dk_T}{\upsilon_1 T_m}\dfrac{\left(T_w-T_\infty\right)}{\left(C_w-C_\infty\right)}$ (Soret Number). *(6)*

3. SHEAR STRESS, NUSSELT AND SHERWOOD NUMBER

All the quantities of chief physical interest are shear stress, Nusselt number and Sherwood number. The following equations represent the local and average shear stress at the plate, local shear stress, (Mahanta and Choudhury (2012))

$$\tau_L=\mu_0\left[\frac{\partial u}{\partial y}+\alpha\left\{\frac{\partial}{\partial y}\left(\frac{\partial u}{\partial t}\right)+v\frac{\partial^2 u}{\partial y^2}\right\}\right]_{y=0} \quad \text{and}$$

average shear stress,

$$\tau_A=\mu_0\int\left[\frac{\partial u}{\partial y}+\alpha\left\{\frac{\partial}{\partial y}\left(\frac{\partial u}{\partial t}\right)+v\frac{\partial^2 u}{\partial y^2}\right\}\right]_{y=0}dx$$

which are proportional to

$$\left[\frac{\partial U}{\partial Y}+\alpha\left\{\frac{\partial}{\partial Y}\left(\frac{\partial U}{\partial \tau}\right)+v\frac{\partial^2 U}{\partial Y^2}\right\}\right]_{Y=0} \quad \text{and}$$

$$\int_0^{100}\left[\frac{\partial U}{\partial Y}+\alpha\left\{\frac{\partial}{\partial Y}\left(\frac{\partial U}{\partial \tau}\right)+v\frac{\partial^2 U}{\partial Y^2}\right\}\right]_{Y=0}dX$$

respectively. From the temperature field, the effects of various parameters on the local and average heat transfer coefficients. The following equations represent the local and average heat transfer rate that is well known Nusselt number, local Nusselt

number, $N_{uL} = \mu_0 \left(\frac{\partial T}{\partial y} \right)_{y=0}$ and average Nusselt number, $N_{uA} = \mu_0 \int \left(\frac{\partial T}{\partial y} \right)_{y=0} dx$ which are proportional to $\left(\frac{\partial \theta}{\partial Y} \right)_{Y=0}$ and $\int_0^{100} \left(\frac{\partial \theta}{\partial Y} \right)_{Y=0} dX$ respectively. And from the concentration field, the effects of various parameters on the local and average mass transfer coefficients. The following equations represent the local and average mass transfer rate that is well known Sherwood number, local Sherwood number, $S_{hL} = \mu_0 \left(\frac{\partial C}{\partial y} \right)_{y=0}$ and average Sherwood number, $S_{hA} = \mu_0 \int \left(\frac{\partial C}{\partial y} \right)_{y=0} dx$ which are proportional to $\left(\frac{\partial \varphi}{\partial Y} \right)_{Y=0}$ and $\int_0^{100} \left(\frac{\partial \varphi}{\partial Y} \right)_{Y=0} dX$ respectively.

4. NUMERICAL SOLUTIONS

The system of non-dimensional, nonlinear, coupled partial differential equations (6) to (9) with boundary condition (10) are solved numerically using explicit finite difference method. To obtain the difference equations, the region of the flow is divided into a grid or mesh of lines parallel to X and Y axes, where X -axis is taken along the plate and Y -axis is normal to the plate.

Here the plate of height $X_{\max}(=100)$ is considered i.e. X varies from 0 to 100 and assumed $Y_{\max}(=35)$ as corresponding to $Y \to \infty$ i.e. Y varies from 0 to 35. There are $m(=180)$ and $n(=180)$ grid spacing in the X and Y directions respectively as shown in Fig. 2.

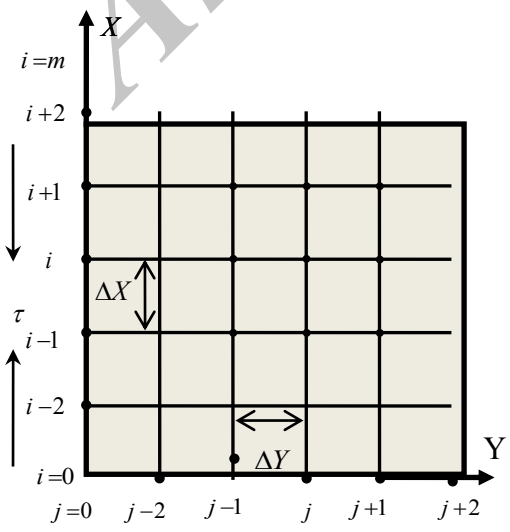

Fig.2.Explicit finite difference system grid.

It is assumed that ΔX, ΔY are content mesh size along X and Y directions respectively and taken as follows, $\Delta X = 0.56(0 \le X \le 100)$ and $\Delta Y = 0.19(0 \le Y \le 35)$ with the smaller time-step, $\Delta \tau = 0.005$.

Let $U', W', \overline{T}'$ and $\overline{C}'$ denote the values of $U, W, \overline{T}$ and $\overline{C}$ are the end of a time-step respectively. Using the explicit finite difference approximation, the following appropriate set of finite difference equations are obtained as;

$$\frac{U'_{i,j} - U'_{i-1,j}}{\Delta X} + \frac{V_{i,j} - V_{i,j-1}}{\Delta Y} = 0 \tag{11}$$

$$\frac{U'_{i,j} - U_{i,j}}{\Delta \tau} + U_{i,j} \frac{U_{i,j} - U_{i-1,j}}{\Delta X} + V_{i,j} \frac{U_{i,j+1} - U_{i,j}}{\Delta Y}$$
$$= G_r \theta_{i,j} + G_m \varphi + \frac{U_{i,j+1} - 2U_{i,j} + U_{i,j-1}}{(\Delta Y)^2} - MU_{i,j} + \alpha \times$$
$$\left\{ \frac{U'_{i,j+1} - U_{i,j+1} - 2U'_{i,j} + 2U_{i,j} + U'_{i,j-1} - U_{i,j-1}}{\Delta \tau (\Delta Y)^2} \right\}$$
$$+ \alpha \left\{ V_{i,j} \left(\frac{U_{i,j+2} - U_{i,j+1} - U_{i,j-1} + U_{i,j}}{(\Delta Y)^3} \right) \right\} \tag{12}$$

$$\frac{\theta'_{i,j} - \theta_{i,j}}{\Delta \tau} + U_{i,j} \frac{\theta_{i,j} - \theta_{i-1,j}}{\Delta X} + V_{i,j} \frac{\theta_{i,j+1} - \theta_{i,j}}{\Delta Y}$$
$$= \frac{1}{P_r} \frac{\theta_{i,j+1} - 2\theta_{i,j} + \theta_{i,j-1}}{(\Delta Y)^2}$$
$$+ D_u \frac{\varphi_{i,j+1} - 2\varphi_{i,j} + \varphi_{i,j-1}}{(\Delta Y)^2} \tag{13}$$

$$\frac{\varphi'_{i,j} - \varphi_{i-1,j}}{\Delta \tau} + U_{i,j} \frac{\varphi_{i,j} - \varphi_{i-1,j}}{\Delta X} + V_{i,j} \frac{\varphi_{i,j+1} - \varphi_{i,j}}{\Delta Y}$$
$$= \frac{1}{S_c} \frac{\varphi_{i,j+1} - 2\varphi_{i,j} + \varphi_{i,j-1}}{(\Delta Y)^2}$$
$$+ S_r \frac{\theta_{i,j+1} - 2\theta_{i,j} + \theta_{i,j-1}}{(\Delta Y)^2} \tag{14}$$

with the boundary condition;

$$U^n_{i,0} = 1,\ \theta^n_{i,0} = 1,\ \phi^n_{i,0} = 1 \tag{15}$$
$$U^n_{i,L} = 0,\ \theta^n_{i,L} = 0,\ \phi^n_{i,L} = 0 \text{ where } L \to \infty$$

Here the subscript i and j designates the grid points with X and Y coordinates respectively and the superscript n represents a value of time, $\tau = n\Delta\tau$ where $n = 0, 1, 2, \ldots\ldots$. The velocity (U), temperature (θ) and concentration (φ) distributions at all interior nodal points have been computed by successive applications of the above finite difference equations. The numerical values of the local shear stresses, local Nusselt number and local Sherwood number are evaluated by **Five-point** approximate formula for the derivatives and then the average shear stress, Nusselt number and Sherwood number are calculated by the use of the **Simpson's**

$\frac{1}{3}$ integration formula. The stability conditions of the methods are $U\frac{\Delta\tau}{\Delta X}+|V|\frac{\Delta\tau}{\Delta Y}+\frac{2}{P_r}\frac{\Delta\tau}{(\Delta Y)^2}\le 1$ and $U\frac{\Delta\tau}{\Delta X}+|V|\frac{\Delta\tau}{\Delta Y}+\frac{1}{S_c}\frac{\Delta\tau}{(\Delta Y)^2}\le 1$. Our solution is valid for the above mentioned conditions. When the value of $\Delta\tau$, ΔX and ΔY approach to zero then the problem will be converged. That's mean the results of the explicit finite difference method approach the true solutions.

5. NUMERICAL SOLUTIONS

To investigate the physical situation of the problem, the numerical values and graphs of velocity (U), temperature (θ) and concentration (φ) distributions as well as shear stress, Nusselt number and Sherwood number within the boundary layer have been computed for different values of Dufour number (D_u), Visco-elastic Parameter (α), Magnetic parameter (M), Prandtl number (P_r), Schmidt number (S_c) and Soret number (S_r) with the help of a computer programming language Compaq Visual Fortran 6.6a and Tecplot 7. These computed numerical results have been shown graphically. To obtain the steady-state solutions, the computation has been carried out up to $\tau=80$. It is observed that the numerical values of U, θ and φ however, show little changes after $\tau=40$. Hence at $\tau=40$ for all variables are steady-state solutions.

The importance of cooling problem in nuclear engineering in connection with the cooling of reactors, the value of the Grashof number for heat transfer is taken to be positive $(G_r>0)$ and the present study has considered $G_r=1.00$. Since the most important fluids are atmospheric air and water, so that the results are limited to $P_r=0.71$ (Prandtl number for air at $20^\circ C$), $P_r=1.00$ (Prandtl number for or salt water)) and $P_r=7.00$ (Prandtl number for water at $20^\circ C$). Here the investigation are assumed for both lighter and heavier fluid particles, hence the values of Schmidt number (S_c) are taken 0.60, 0.78 and 1.00 (in particular, 0.60 for water vapor that represents a diffusing chemical species of most common interest in air, 0.78 for ammonia and 1.00 for carbon dioxide) which represent the specific condition of the flow. However the values of other parameters are chosen arbitrarily and also the modified Grashof number $G_m=1.00$ for mass transfer are considered as a fixed value.

To observe the physical situation of the problem, the solutions have been illustrated in Figs. 3 to 33. The velocity profiles have been displayed for various values of Dufour number (D_u), Magnetic parameter (M), Prandtl number (P_r), Schmidt number (S_c) and Soret number (S_r) respectively in Figs. 3 to 7. These results show that the velocity increases with the increase Dufour number, Soret number and decreases with the increase Prandtl number, Schmidt number, Magnetic parameter respectively.

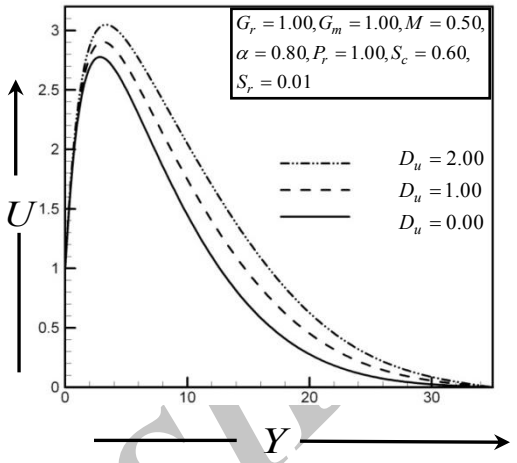

Fig. 3. Velocity profile for different values of Dufour number, D_u.

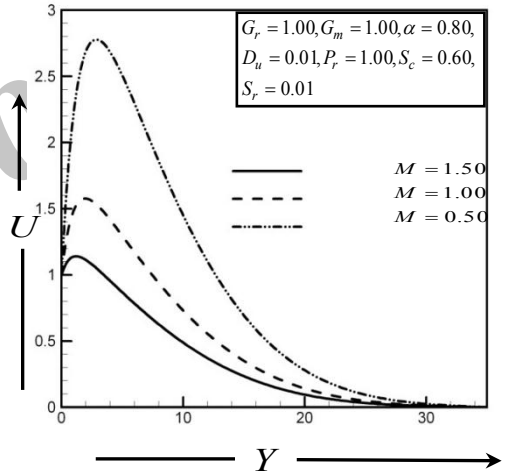

Fig. 4. Velocity profile for different values of Magnetic parameter, M.

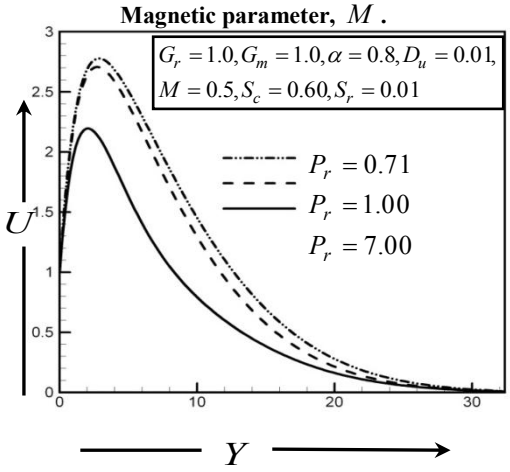

Fig. 5. Velocity profile for different values of Prandtl number, P_r.

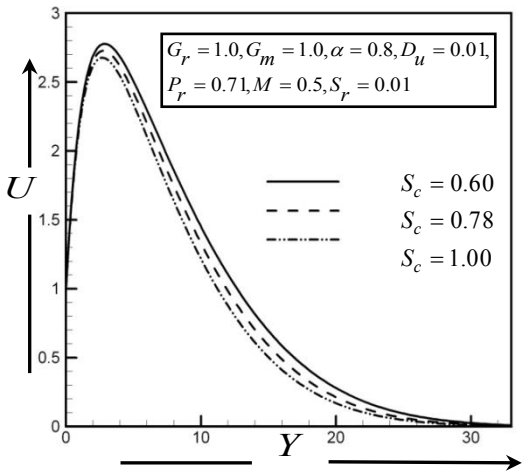

Fig. 6. Velocity profile for different values of Schmidt number, S_c ..

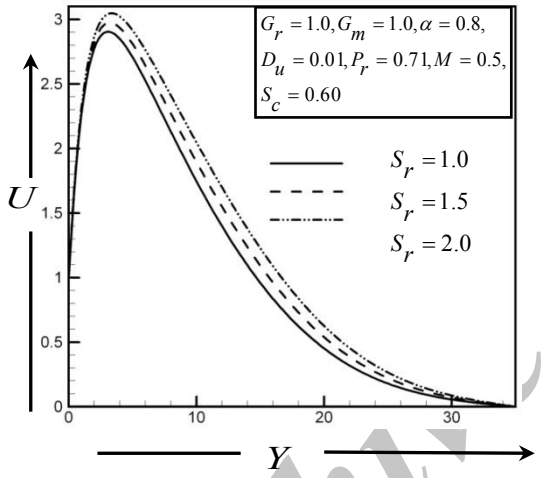

Fig. 7. Velocity profile for different values of Schmidt number, S_r .

The temperature distributions have been illustrated for various values of Dufour number (D_u) and Prandtl number (P_r) respectively in Figs. 8 and 9. These results show that the temperature distributions increase with the increase Dufour number and decrease for the increase Prandtl number respectively. The concentration profiles have been shown for various values of Schimdt number (S_c) and Soret number (S_r) respectively in Figs. 10 and 11. These results show that the concentation distributions increase with the increase Soret number and decrease for the increase Schmidt number respectively.

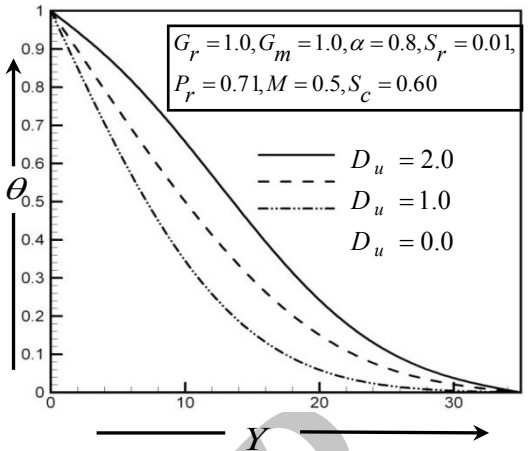

Fig. 8. Temperature profile θ for different values of Dufour number, D_u .

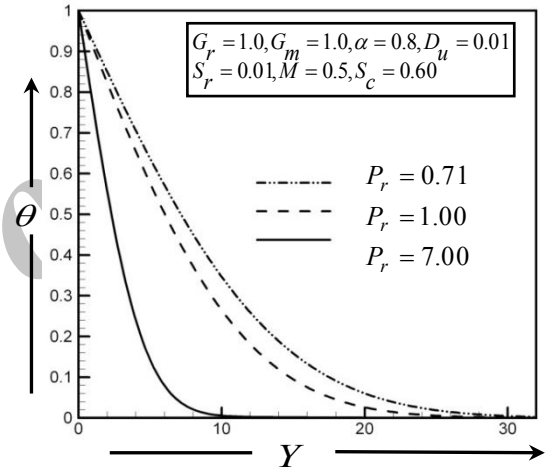

Fig. 9. Temperature profile for different values of Prandtl number, P_r .

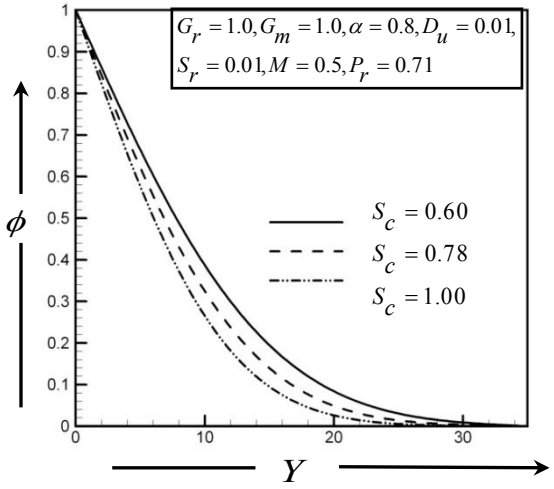

Fig. 10. Concentration profile for different values Schmidt number, S_c .

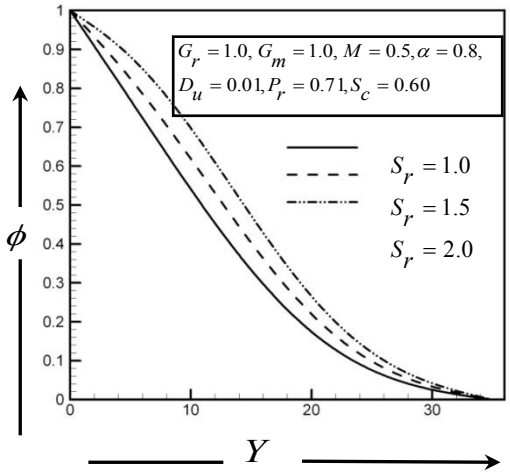

Fig. 11. Concentration profile for different values Soret number, S_r.

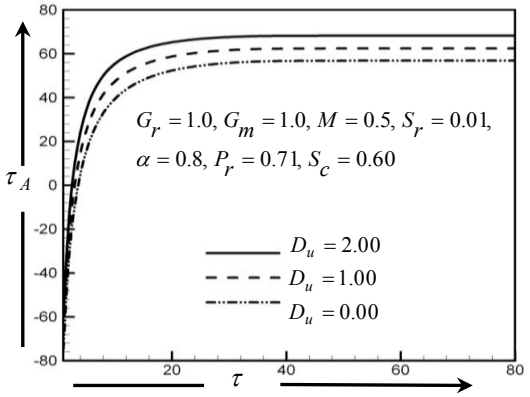

Fig. 12. Average shear stress for different values of Dufour number, D_u.

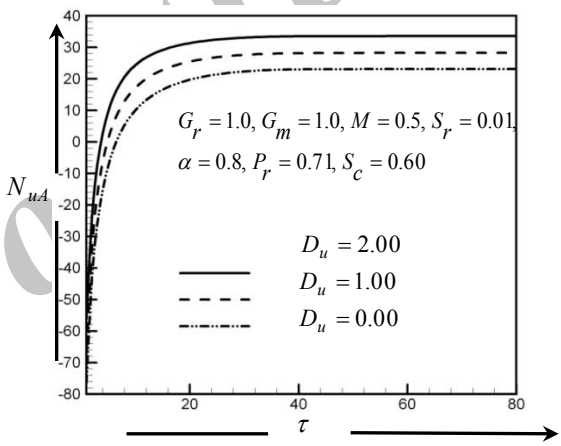

Fig. 13. Average Nusselt number for different values of Dufour number, D_u.

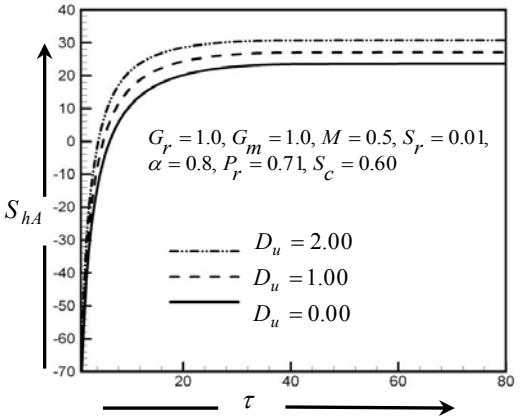

Fig. 14. Average Sherwood number for different values of Dufour number, D_u.

Figures. 12 to 14 show the average shear stress, Nusselt number and Sherwood number for various values of Dufour number (D_u). The average shear stress, Nusselt number and Sherwood number increase with the increase of Dufour number. The average shear stress, Nusselt number and Sherwood number have been displayed for various values of Magnetic parameter (M) in Figs. 15 to 17, Prandtl number (P_r) in Figs. 18-20, Schmidt number (S_c) in Figs. 21 to 23 and Soret number (S_r) in Figs. 24 to 26 respectively. The average shear stress, Nusselt number and Sherwood number deccrease with the increase of Magnetic parameter, Prandtl number, Schmidt number and decrease with the increase of Soret number.

Local shear stress decreases with the increase of Visco-elastic parameter. The local shear stress and Nusselt number have been illustrated for various values of Dufour Number (D_u) in Figs. 27 and 28. Local shear stress and Nusselt number increase with the increase of Dufour Number. In Fig. 29 displays the local shear stress for various values of Magnetic parameter (M). The local shear stress decreases with the increase of Magnetic parameter. Figs. 30 and 31 show the local shear stress and Nusselt number for various values of Prandtl number (P_r). The local shear stress and Nusselt number decrease with the increase of Prandtl number. Local Sherwood number has been displayed in Fig. 32 for various values of Schmidt number (S_c) and in Fig. 33 for various values of Soret number (S_r). The local Sherwood number decreases with the increase of Schmidt number and increases with increases of Soret number.

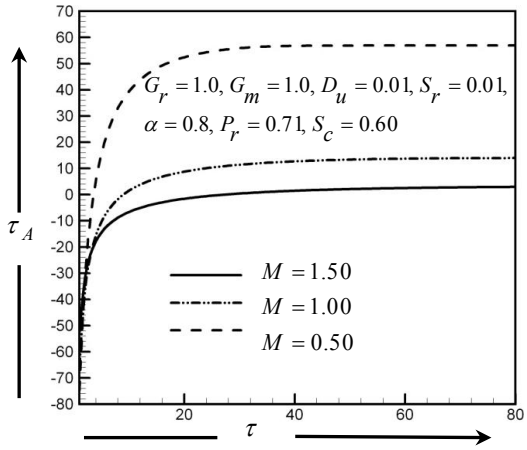

Fig. 15. Average Shear stress for different values of Magnetic parameter, M .

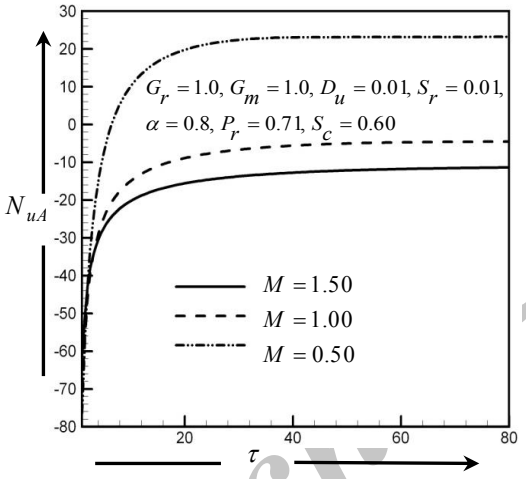

Fig. 16. Average Nusselt number for different values of Magnetic parameter, M .

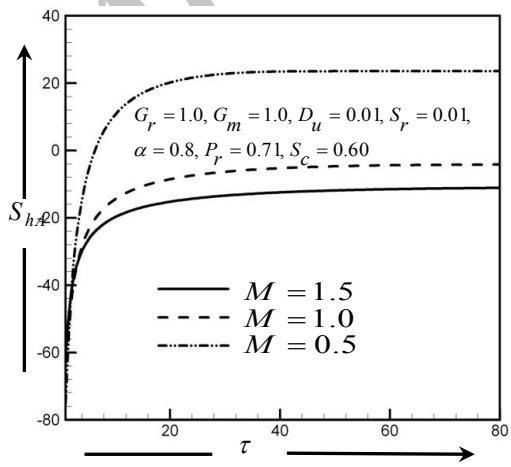

Fig. 17. Average Sherwood number for different values of Magnetic parameter, M .

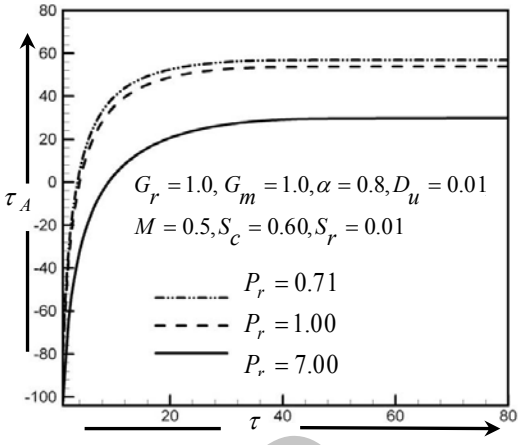

Fig. 18. Average Shear stress for different values of Prandtl number, P_r .

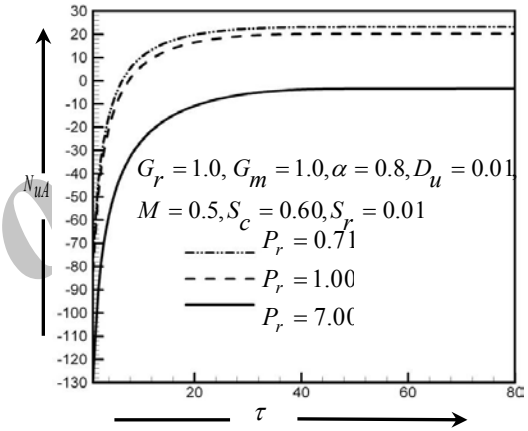

Fig. 19. Average Nusselt number for different values of Prandtl number, P_r .

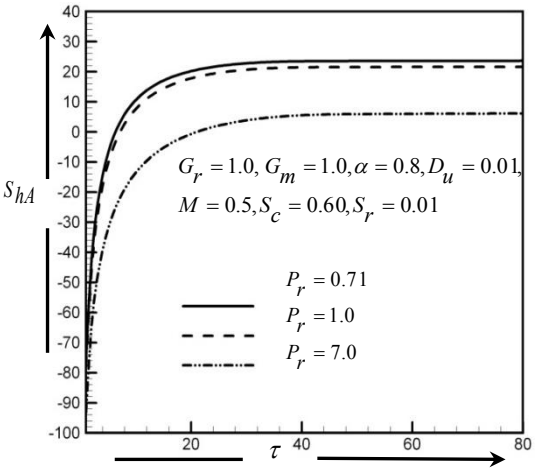

Fig. 20. Average Sherwood number for different values of Prandtl number, P_r .

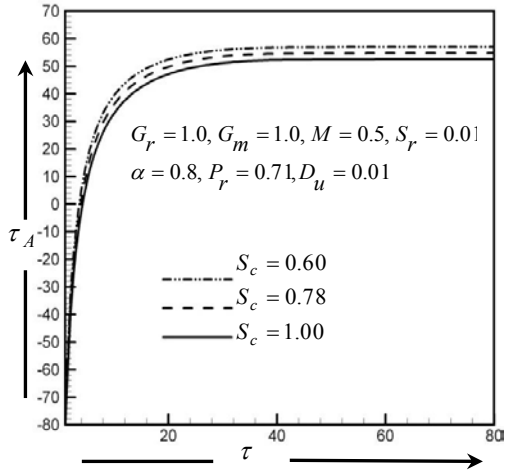

Fig. 21. Average Shear stress for different values of Schmidt number, S_c .

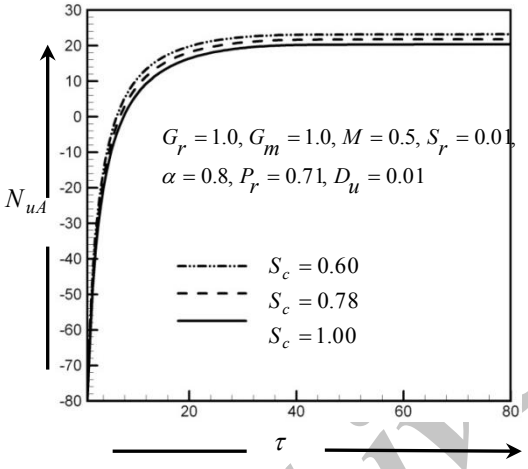

Fig. 22. Average Nusselt number for different values of Schmidt number, S_c .

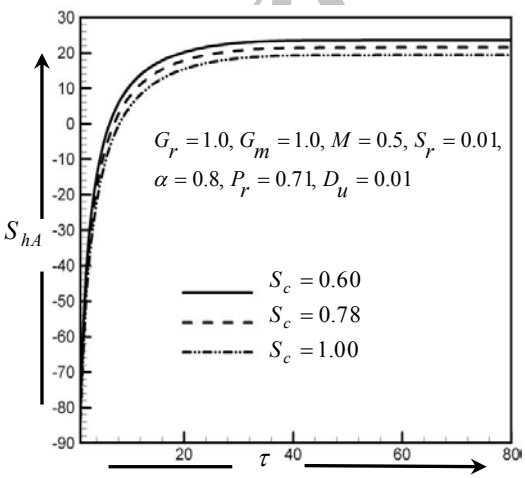

Fig. 23. Average Sherwood number for different values of Schmidt number, S_c .

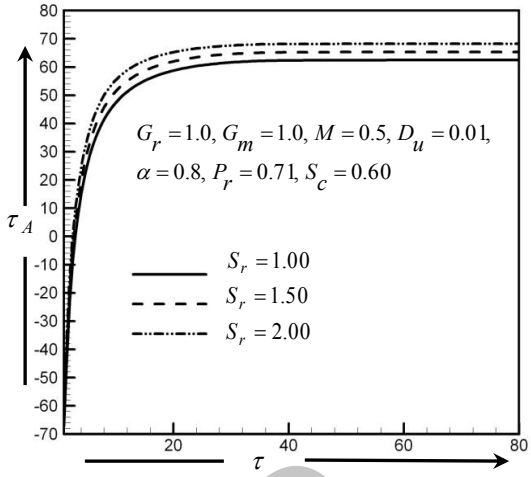

Fig. 24. Average Shear stress for different values of Soret number, S_r .

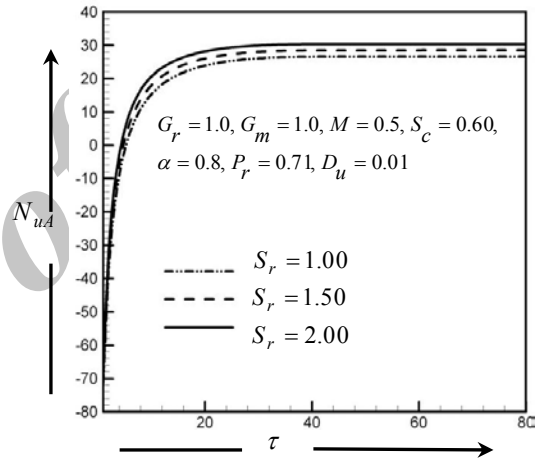

Fig. 25. Average Nusselt number for different values of Soret number, S_r .

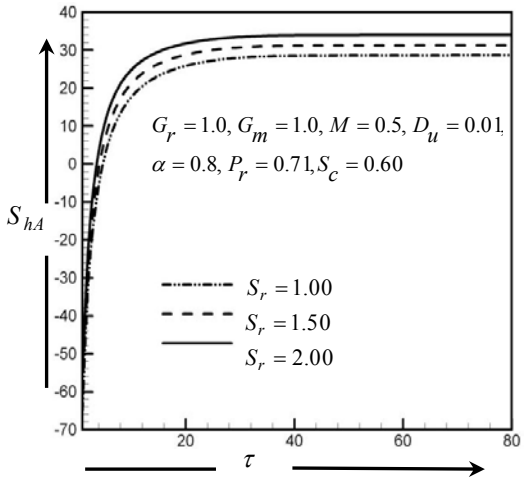

Fig. 26. Average Sherwood number for different values of Soret number, S_r .

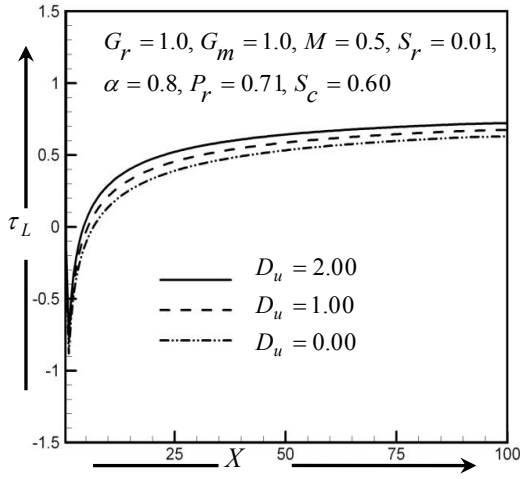

Fig. 27. Local shear stress for different values of Dufour number, D_u .

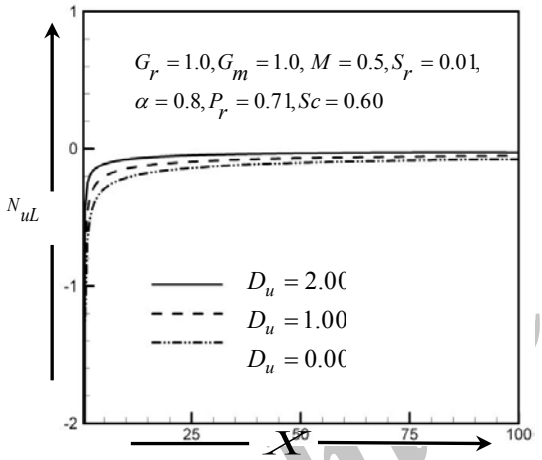

Fig. 28. Local Nusselt number for different values of Dufour number, D_u .

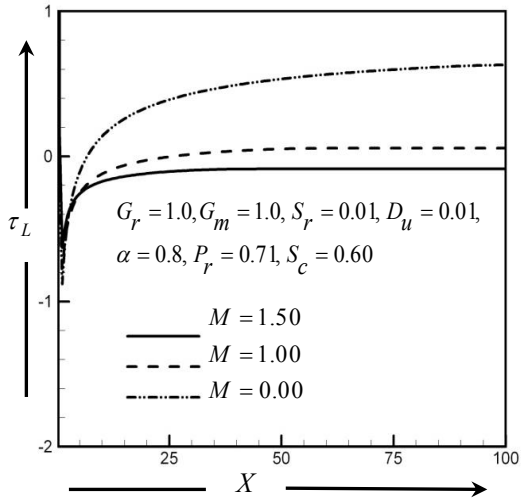

Fig. 29. Local shear stress for different values of Magnetic parameter, M .

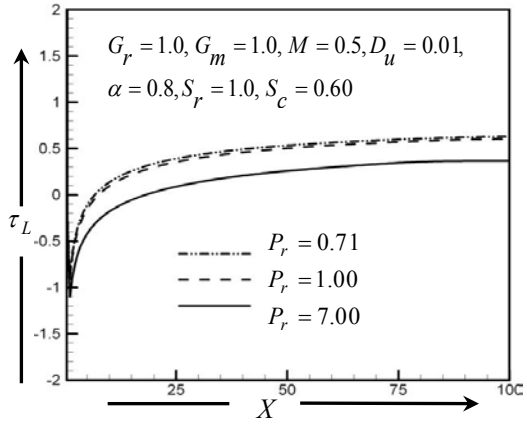

Fig. 30. Local shear stress for different values of Prandtl number, P_r .

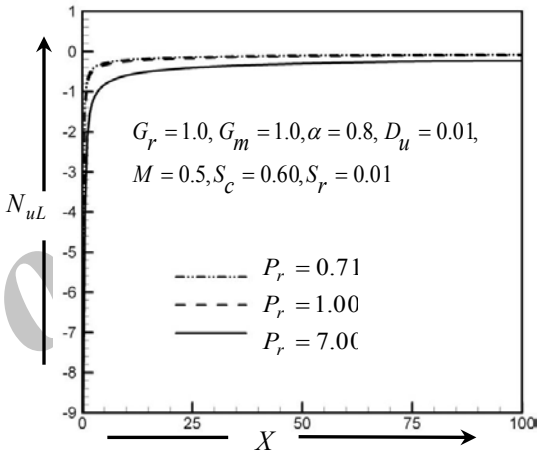

Fig. 31. Local Nusselt number for different values of Prandtl number, P_r .

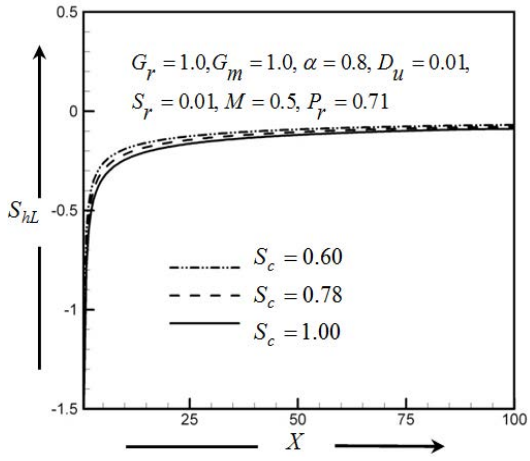

Fig. 32. Local Sherwood number for different values of Schmidt number, S_c .

Finally, a qualitative comparison of the present steady-state results with the published results (Gbadeyan *et al*. (2011)) is presented in Table. 1. The accuracy of the present results is qualitatively good in case of all the flow parameters

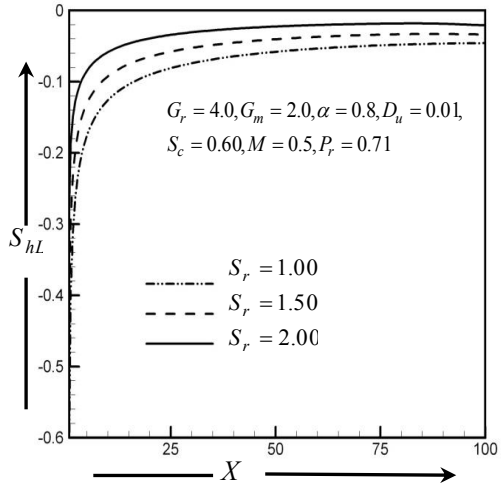

Fig. 33. Local Sherwood number for different values of Soret number, S_r .

6. CONCLUSION

In this study, the finite difference solution of unsteady diffusion-thermo and thermal-diffusion effects on MHD Visco-elastic fluid flow over a vertical plate is investigeted. Important findings of this investigation are given below;

1. The velocity profiles increase with the increase of Dufour number and Soret number and reverse effect with the increase of Magnetic parameter, Prandtl number and Schmidt number.

2. The temperature distributions increase with the increase of Dufour number and reverse effect with the increse of Prandtl number.

3. The concentration profiles decrease with the increase of Schmidt number reverse effects with the increse of Soret number.

It is expected that the findings of this investigation may be useful for study of movement oil or gas and water through the reservoir of an oil or gas field, in the migration of underground water or oil as well as in the filtration and water purification processes, the findings may be useful for study of movement of oil or gas and water through the reservoir of an oil or gas field. These results may also be useful for plasma studies as well as in power engineering, geothermal energy extractions, geophysics and astrophysics.

Table 1 Qualitative comparison of the present results with the previous results

Increased Parameter	Previous results given by Gbadeyan *et al.* (2011)			Present results								
	u	θ	ϕ	U	θ	φ	τ_L	τ_A	N_{uL}	N_{uA}	S_{hL}	S_{hA}
D_u	Inc.	Inc.		Inc.	Inc.		Inc.	Inc.	Inc.	Inc.		Inc.
M	Dec.			Dec.			Dec.	Dec.		Dec.		Dec.
P_r		Dec.		Dec.	Dec.		Dec.	Dec.	Dec.	Dec.	Dec.	Dec.
S_c				Dec.		Dec.		Dec.		Dec.		Dec.
S_r			Inc.	Dec.		Inc.		Inc.		Inc.	Inc.	Inc.

REFERENCES

Chowdhury, M. K. and M. N. Islam (2000). MHD free convection flow of visco-elastic fluid past an infinite vertical porous plate. *Heat and Mass Transfer* 36, 439.

Gbadeyan, J. A., A. S. Idowu, A. W. Ogunsola, O. O. Agboola and P.O. Olanrewaju (2011). Heat and mass transfer for Soret and Dufour's effect on mixed convection boundary layer flow over a stretching vertical surface in a porous medium filled with a viscoelastic fluid in the presence of magnetic field. *Global Journal of Science Frontier Research* 11(8), 97-114.

Hayat, T., M. Mustafa and I. Pop (2010). Heat and mass transfer for Soret and Dufour's effect on mixed convection boundary layer flow over a stretching vertical surface in a porous medium filled with a viscoelastic fluid. *Communications in Nonlinear Science and Numerical Simulation* 15(9), 1183-1196.

Hussaini, S. A., M. V. R. Murthy, A. Waheedullah and Rafiuddin (2013). MHD Unsteady

Memory Convective Flow through Porous Medium with Variable Suction. *Journal of Applied Fluid Mechanics* 6(2), 197-202.

Mahanta, M. and R. Choudhury (2012). Mixed convective MHD flow of visco-elastic fluid Past a vertical infinite plate with mass transfer. *International Journal of Scientific & Engineering Research* 3(2), 1-7.

Nanousis, N (1992). Unsteady Magnetohydrodynamic flows in a rotating elasto-viscous fluid. *Astrophysics and Space Science* 199(2), 1183-1196.

Rajesh, V. and S. V. K. Varma (2010). Radiation effects on MHD flow through a porous medium with variable temperature or variable mass diffusion. *International Journal of Applied. Math and Mech* 6(1), 39-57.

Rajesh, V. (2011). Heat source and mass transfer effects on MHD flow of an elasto-viscous fluid through a porous medium. *International Journal of Engineering* ,2, 205-212.

Samria, N. K., R. Prasad and M. U. S. Reddy (1990). MHD free convection flow of an elasto-viscous fluid past an infinite vertical plate. *Astro Physics and Space Science* 181, 125-134.

Soundalgekar, V. M. and P. Puri (1969). On Fluctuating Flow of an Elastico-Viscous Fluid Past an Infinite Plate with Variable Suction. *Journal of Fluid Mechanics* 35(3), 561-573.